Physical characterization of glacial rock flours from fjord deposits in South Greenland–Toward soil amendment

Pesch, Charles; Weber, Peter Lystbæk; Moldrup, Per; de Jonge, Lis Wollesen; Arthur, Emmanuel; Greve, Mogens Humlekrog

Published in:
Soil Science Society of America Journal

DOI (link to publication from Publisher):
10.1002/saj2.20352

Publication date:
2022

Document Version
Publisher's PDF, also known as Version of record

ASA, CSSA, and SSSA Virtual Issue Call for Papers:

Advancing Resilient Agricultural Systems: Adapting to and Mitigating Climate Change

Content will focus on resilience to climate change in agricultural systems, exploring the latest research investigating strategies to adapt to and mitigate climate change. Innovation and imagination backed by good science, as well as diverse voices and perspectives are encouraged. Where are we now and how can we address those challenges? Abstracts must reflect original research, reviews and analyses, datasets, or issues and perspectives related to objectives in the topics below. Authors are expected to review papers in their subject area that are submitted to this virtual issue.

Topic Areas

- Emissions and Sequestration
  - » Strategies for reducing greenhouse gas emissions, sequestering carbon
- Water Management
  - » Evaporation, transpiration, and surface energy balance
- Cropping Systems Modeling
  - » Prediction of climate change impacts
  - » Physiological changes
- Soil Sustainability
  - » Threats to soil sustainability (salinization, contamination, degradation, etc.)
  - » Strategies for preventing erosion
- Strategies for Water and Nutrient Management
  - » Improved cropping systems
- Plant and Animal Stress
  - » Protecting germplasm and crop wild relatives
  - » Breeding for climate adaptations
  - » Increasing resilience
- Waste Management
  - » Reducing or repurposing waste
- Other
  - » Agroforestry
  - » Perennial crops
  - » Specialty crops
  - » Wetlands and forest soils

Climate Change Virtual Issue

Submit Now!

Deadlines

Abstract/Proposal Deadline: Ongoing
Submission deadline: 31 Dec. 2022

How to submit

Submit your proposal to manuscripts@sciencesocieties.org

Please contact Jerry Hatfield at jerryhatfield67@gmail.com with any questions.

American Society of Agronomy | Crop Science Society of America | Soil Science Society of America

Received: 6 July 2021 | Accepted: 4 November 2021 | Published online: 24 January 2022

DOI: 10.1002/saj2.20352

Soil Science Society of America Journal

PEDOLOGY

Physical characterization of glacial rock flours from fjord deposits in South Greenland–Toward soil amendment

Charles Pesch[1] | **Peter Lystbæk Weber**[2] | **Per Moldrup**[1] | **Lis Wollesen de Jonge**[2] | **Emmanuel Arthur**[2] | **Mogens Humlekrog Greve**[2]

[1] Dep. of the Built Environment, Aalborg Univ., Thomas Manns Vej 23, DK-9220, Aalborg, Denmark

[2] Dep. of Agroecology, Aarhus Univ., Blichers Allé 20, P.O. Box 50, DK-8830, Tjele, Denmark

Correspondence
Charles Pesch, Dep. of the Built Environment, Aalborg Univ., Thomas Manns Vej 23, DK-9220, Aalborg, Denmark.
Email: cmep@build.aau.dk

Assigned to Associate Editor Travis Nauman.

Funding information
Teknologi og Produktion, Det Frie Forskningsråd, Grant/Award Number: 8022-00184B

Abstract

Greenlandic fjords contain vast amounts of glacially derived mineral material (glacial rock flour [GRF]), which may be used to amend structureless, low-clay, and water-repellent agricultural soils in South Greenland and elsewhere. In this study, we investigate key physical amendment properties of GRF from 16 different deposits in South Greenland. The clay-sized fraction varied largely (range, 0.11–0.57 kg kg^{-1}), and the particles were mostly angular. The specific surface area (SSA) determined by either ethylene glycol monomethyl ether (EGME, polar liquid) (range, 13.32–88.06 m^2 g^{-1}) or water-vapor adsorption (range, 10.62–63.82 m^2 g^{-1}) agreed well (r = .90) and were comparable to kaolinitic-clay dominated cultivated soils (KA-soils) with clay content similar to the GRFs. The cation exchange capacities (CECs) (range, 4.25–21.91 cmol kg^{-1}) were similar to or higher than those of the KA-soils. The water content at the permanent wilting point (PWP) for the GRFs were considerably lower than those of the KA-soils. The addition of 5% GRF to a sandy soil from Greenland showed a tendency (although not statistically significant) to increase plant available water (PAW). However, very high GRF addition (10 and 15%) significantly decreased the PAW. The specific surface charge (CEC/SSA) of the GRFs were higher than for comparable KA-soils, suggesting a good soil amendment potential. The results from this study are valuable toward designing sustainable GRF amendment strategies, matching a given cultivated soil with the right amount and type of GRF.

1 | INTRODUCTION

The South Greenlandic soils are characterized by a relatively coarse texture and moderate to high organic matter (OM) content and show little to moderate soil development (Jakobsen, 1991); Caviezel et al., 2017; Weber et al., 2020; Pesch et al., 2021). In a recent study, Weber et al. (2021) revealed the hydrophobic tendency of Greenlandic agricultural soils, which was attributed to the combination of coarse soil texture and high OM content. Furthermore, Pesch et al.

Abbreviations: CEC, cation exchange capacity; DSL, Danish Soil Library; EC, electrical conductivity; EGME, ethylene glycol monomethyl ether; GRF, glacial rock flour; IL, illite; KA, kaolinite; KA-soils, kaolinitic-clay-dominated cultivated soils; LD, laser diffraction; MO, montmorillonite; OM, organic matter; PAW, plant available water; PSD, particle size distribution; PWP, permanent wilting point; RH, relative humidity; SP, sieve and pipette; SSA, specific surface area; SSA_w, specific surface area estimated from water vapor sorption isotherms; SSC, specific surface charge; WSI, water vapor sorption isotherm; Ψ, soil-water potential

(2021) revealed the quasi absence of any soil aggregation and Weber et al. (2020) pointed out the complexity of adequate soil aeration because of pronounced pore network tortuosity. The cold environment, relatively coarse soil texture, and the lack of soil development result in large amounts of noncomplexed OM (Pesch et al., 2020), which will be prone to degradation following increasing temperatures (Kirschbaum, 1995) or changes in soil management (Besnard et al., 1996).

To counteract such unfavorable soil conditions for productive agriculture, different soil amelioration strategies have shown more or less promising results (Maslov, 2009). Intentional or unintentional soil conditioning has a long history in agriculture (Simonson, 1959), and in recent years, the use of chemically untreated mineral rock dust has been given more attention (van Straaten, 2007).

It is well known that the soil's fine particle content governs its functional, physical, and chemical properties. Among others, McKissock et al. (2002) reported that the addition of small amounts of clay (≤1.6% w/w) effectively reduced water repellency in sandy soils even though for coarse soils, the finer fractions often exhibit highest water repellency because of the higher OM content of the finer fractions (de Jonge et al., 1999). This corroborates with Tahir and Marschner (2016), who reported increased OM retention in Australian farmlands after clay amendment. Dexter et al. (2008), Schjønning et al. (2010), Oades (1984), and Wagner et al. (2007) pointed out the importance of the specific surface area (SSA) and thus the content of fine particles of the mineral soil fraction for OM protection and soil aggregate stability. The soil's nutrient holding capacity is largely dependent on the OM and the fine mineral fraction and the associated cation exchange capacity (CEC), as concluded by Matus (2021) and Nguyen and Marschner (2013). Last but not least, the effect of the fine solid fraction on soil-water retention and plant-available water is widely acknowledged (e.g., Rawls & Brakensiek, 1982; Karup et al., 2017).

Throughout the former glaciated parts of the northern hemisphere, the perpetual movement of the ice sheet produced vast amounts of fine-grained mineral material by abrading the crystalline bedrock with debris embedded in its basement (Belmonte, 2015). The sediments were discharged via the glacial outwash streams into periglacial lakes or into the marine environment, where the particles settled and formed thick bottom layers of fine-grained material, referred to as glacial rock flour (GRF). Investigations on sediments originating from Alaska (Ramesh & D'Anglejan, 1995), Canada (Bentley & Smalley, 1979), Scandinavia (Roaldset, 1972), and South Greenland (Belmonte, 2015) revealed that they shared similar mineralogical properties with varying clay content between 20 and 90% (w/w). Under specific circumstances, the low internal cohesion of the sediments of the raised seabeds can lead to dangerous landslides and serious subsidence; therefore, their geotechnical properties have been investigated in detail (Belmonte, 2015). Generally, the abraded and mechanically weathered mineral material mainly consisted of the primary minerals quartz, feldspars, and amphiboles, which were also found in relatively high abundances in the clay fraction (<2 μm). Pederstad and Jørgensen (1985) and Belmonte (2015) reported the presence of illite and kaolinite in the clay-sized fraction as well as expandable clays (e.g., smectite and vermiculite) and concluded that the material underwent subaerial postglacial chemical weathering.

Core Ideas

- We analyzed fine-grained, glacially abraded mineral material from Greenland.
- The surface area was comparable with similar-textured, kaolinitic-clay-dominated soils (KA-soils).
- The water content at the permanent wilting point was lower than that of KA-soils.
- The cation exchange capacity was similar to or higher than that of KA-soils
- The properties of the glacial rock flour suggest that it can be used as mineral soil amendment.

There are only a few studies that investigated the use of Greenlandic GRF as a potential soil fertilizer. Gunnarsen et al. (2019) applied GRF as mineral fertilizer in controlled laboratory experiments and concluded that the GRF could act as slow-release potassium and magnesium source for crops. Furthermore, Gunnarsen (2020) concluded that high rates of GRF application increased biomass production in active soil environments following enhanced weathering of the mineral material. Sukstorf et al. (2020) presented the results of a one-season (2 mo) field experiment in Greenland and concluded that an amendment with only GRF was not suited as short-term fertilizer; however, a combination of GRF and artificial N–P–K fertilizer significantly increased the yields. Regarding the slow dissolution rates of the primary silicates found in the GRF, especially in cold environments, the results of Sukstorf et al. (2020) were expected. In contrast to conventional soil amendments, for example, organic and artificial fertilizers, or liming, the addition of a fine-grained mineral material to soil is a long-term and profound intervention on the soil, and any negative effect on the latter needs to be assessed before large-scale application.

This study is a first step toward the availability and characterization of GRF deposits across South Greenland in the perspective of their suitability as soil conditioner for the local farmland. The focus was put on potential soil–GRF interactions after application to (a) promote soil development in terms of aggregation and structure development, (b) increase

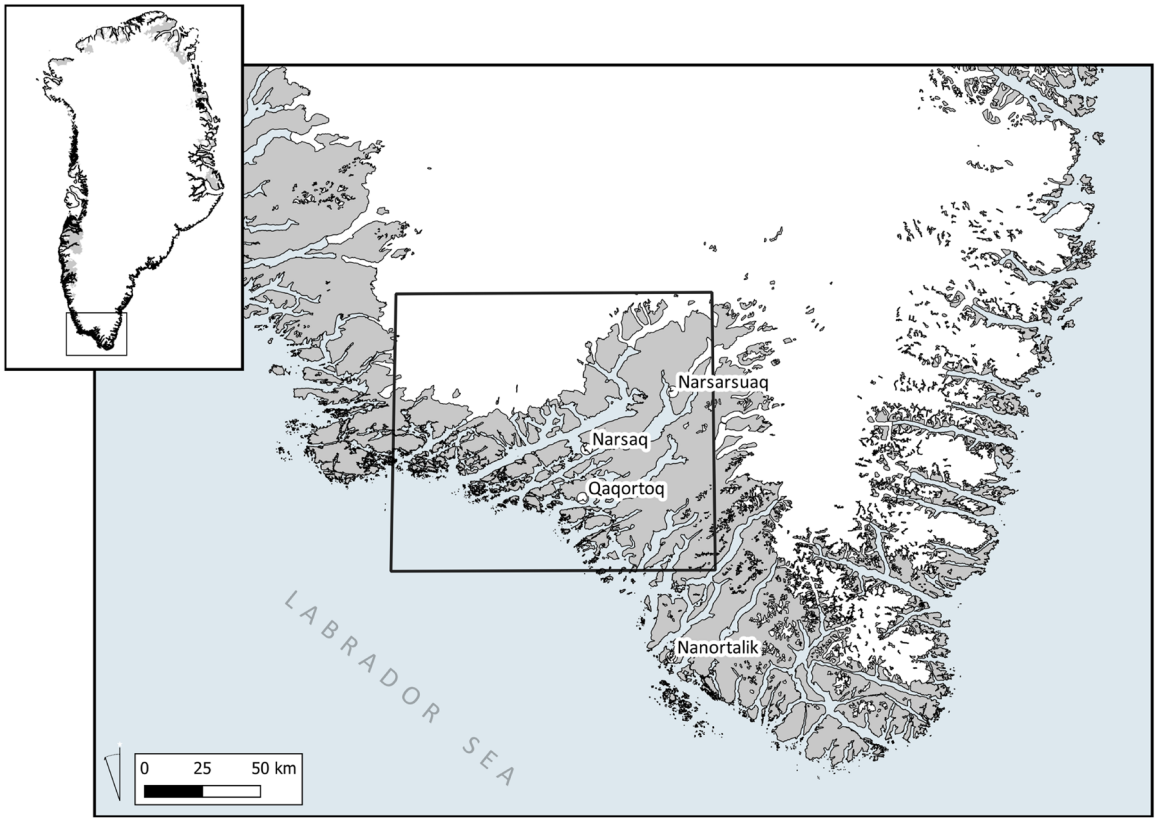

FIGURE 1 Overview of the investigated area in South Greenland. Detailed map of the marked area in Figure 2

mineral fertilizer efficiency, and (c) exclude negative effects on water-holding capacity. For this purpose, we analyzed the particle-size distribution, the SSA, and CEC of 16 selected GRF deposits found in the vicinity of the present agricultural area in South Greenland. Additionally, the bulk mineralogy and several basic soil chemical and physical properties were determined and discussed.

2 | MATERIAL AND METHODS

2.1 | Geological description of the study area

The investigated area (Figure 1) lies within the diverse geological Gardar province, which formed 1.2 Ga BP. It is surrounded by the Ketilidian fold belt (1.8 Ga) and joins the Archaean block further north (3.8 Ga). The crystalline bedrock (Julianehåb batholith) mainly consists of biotite and hornblende-bearing granite and gneiss (Berrangé, 1966) bearing intrusions of intermediate metavolcanic rocks (plagioclase phenocrysts) and light-colored, small-grained granites (leucocratic quartzo-feldspathic and aplitic rocks) (Kalsbeek et al., 1990). The GRF studied here thus consists of some of the oldest geological surface materials on Earth (Henriksen, 2008).

Agriculture in Greenland mainly consists of sheep husbandry with summer pastures and indoor production during winter. The region is the only important agriculturally exploited area in Greenland totaling ~1,100 ha of occasionally cultivated lands (Westergaard-Nielsen et al., 2015) mainly used for winter fodder production.

The subglacial watersheds encompass large areas, and the abraded mineral material suspended in the outwash streams is thus a mix of the bedrock found throughout the watershed. This assumption corroborates with the findings of Andrews (2011) and White et al. (2016), who investigated the mineralogy of marine sediments along the west coast of Greenland. They reported a general similarity of the mineral composition of the collected samples, which suggests that the sediments originate from a similar parent material.

The formation of the investigated GRF deposits took place in the estuaries of the glacial outwash streams (Bennike et al., 2019; Andrews, 2011) and appeared at the surface only after the isostatic rebound because of reduced load following deglaciation. Considerable continental uplift occurred since the end of the Pleistocene (~11 ka BP), with 20–40 m close to the current inland ice margin (inner-fjord) and 60–80 m in the outer-fjord regions (Bennike et al., 2002). According to Bennike et al. (2002), most of the investigated area was deglaciated prior to 10 ka BP. With time, the deposits were covered by combined solifluction of slope deposits and fluvial and aeolian sediments and thus partly protected from extensive erosion (see photograph in Figure 2).

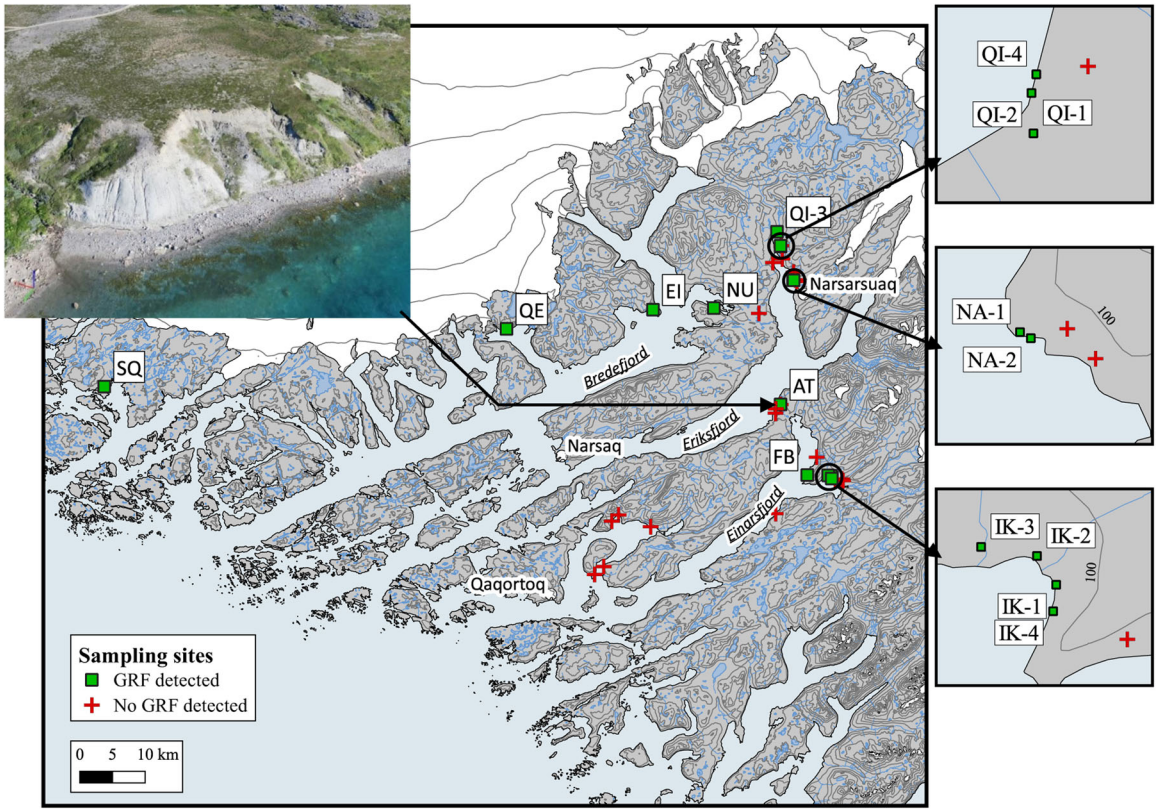

FIGURE 2 Detailed map of the area marked in Figure 1. The approved and discarded sampling sites (green squares and red crosses, respectively) in South Greenland. Top left photograph shows deposition Ataarnasit (AT); its horizontal extent covers ~250 m. EI, Eqaluit Ilulat; FB, Fox Bay; GRF, glacial rock flour; IK, Iterlak; NA, Narsarsuaq; NU, Nunakullak; QE, Qeqertaasaq; QI, Quinngua; SQ, Sioraq

In this study, a total of 16 GRF deposits were either identified from aerial images or reported from locals and sampled during two sampling campaigns in 2018 and 2019 (see map in Figure 1).

We used two datasets from literature as comparative material: the Danish Soil Library (DSL), consisting of 41 agricultural top- and subsoils from Denmark (Hansen, 1976; Resurreccion et al., 2011), and 18 soil samples that have differing clay mineralogy from across the United States and Denmark (Arthur et al., 2020).

2.2 | Laboratory methods

Prior to the laboratory analyses, the air-dry material was carefully crushed in a mortar and presieved to <2 mm. Generally, we found little to no particles >2 mm in the untreated material.

2.2.1 | Texture and organic matter

The texture was determined using a combination of wet sieving and pipette (SP), according to Gee and Or (2002). For total carbon determination, the samples were ball-milled before oxidization of the carbon at 950 ˚C using an elemental analyzer combined with a thermal conductivity detector (Thermo Fisher Scientific) (Nelson & Sommers, 1996). No carbonates were detected; the total carbon could be set equal to the total organic carbon. The OM was obtained by multiplying the total organic carbon with a conversion factor set to 2 as suggested by Pribyl (2010).

The particle size distribution (PSD) was additionally determined by laser diffraction (LD), using a Hydro 2000MU wet dispersion unit coupled to a Mastersizer 2000 (Malvern Instruments Ltd). The samples were dispersed using 0.1 M tetrasodium pyrophosphate ($Na_4P_2O_7$). Further dispersion was achieved by sonication for a period of 60 s. The recorded diffraction pattern was evaluated by the built-in software, using the Mie-scattering theory for which the real and imaginary parts of the refractive index were set to 1.53 and 0.1, respectively, as suggested by Ryżak and Bieganowski (2011). The software stored the result as frequency distribution from which the cumulative PSD was calculated.

2.2.2 | Scanning electron microscopy for particle shape analysis

The shape of the fine fraction of the studied material was visualized by scanning electron microscopy. The pictures were

taken on the air-dried and presieved (<2 mm) material using a Zeiss EVO 60 (Carl Zeiss AG). No additional sample treatments prior to the measurement were performed.

2.2.3 | X-ray diffraction for mineral phase identification

The mineralogical composition of the sediments was determined by X-ray (Cu Kα, 40 mA, 45 kV) powder diffraction analysis (XRD) on the bulk samples using a Malvern Panalytical Empyrean diffractometer mounted with a PIXcel1D detector (Malvern Instruments Ltd). Prior to the measurement, the material was carefully ground in a mortar. No standard for quantitative analysis was added. The step size was set to 0.02 Å with an exposure time of 60 s per step. The semiquantitative mineral phase distribution was determined by Rietveld full-pattern refinement for 2θ degrees ranging from 5 to 65° using the software *Profex* (Doebelin & Kleeberg, 2015).

2.2.4 | Specific surface area and water vapor sorption isotherms

The SSA was determined by the standard ethylene glycol monomethyl ether (EGME) method according to Petersen et al. (1996) and referred to as SSA_{EGME} ($m^2\ g^{-1}$) throughout the text.

The water vapor sorption isotherms (WSIs) were determined using a vapor sorption analyzer (METER Group Inc.). Arthur et al. (2014) include detailed information about the device and procedure. The SSAs were estimated from the WSIs following the procedures as described in the section below and referred to as SSA_w.

2.2.5 | Supporting physical–chemical parameters

The total CEC (cmol kg^{-1}) was measured using the ammonium acetate extraction method according to Sumner and Miller (1996). The acidity of the sediments was assessed by the hydrogen ion activity (pH) measured by a glass electrode on a 1:4 soil/water (pH_w) and soil–0.01 M $CaCl_2$ (pH_{CaCl2}) suspension according to Thomas (1996). The electrical conductivity (EC, μS cm^{-1}) as a measure of salinity was determined with a conductivity cell on a 1:9 soil/water suspension according to Rhoades (1996). The specific surface charge (SSC, cmol m^{-2}) was calculated as the ratio of CEC to SSA_{EGME}.

2.3 | Water vapor sorption isotherm model

The Guggenheim–Anderson–de Boer model (van den Berg & Bruin, 1981), as given in Equation 1, was fitted to the desorption WSIs for water activities (a_w) ranging from 0.2 to 0.8, corresponding to relative humidities (RHs) between 20 and 80% as suggested by Akin and Likos (2014) and Arthur et al. (2018).

$$\theta_m = \frac{\theta_0 \times C \times K \times a_w}{\left[\left(1 - K \times a_w\right)\left(1 - K \times a_w + K \times C \times a_w\right)\right]} \quad (1)$$

where θ_m is the gravimetric water content, θ_0 is the free-fitting parameter representing the gravimetric water content at monolayer coverage, and C and K are related to the thermodynamics of the liquid–solid interactions.

The SSA could eventually be determined from the relation between θ_0 (kg kg^{-1}), the surface covered by one water molecule ($A = 10.8 \times 10^{-20}$), Avogadro's constant ($N_a = 6.02 \times 10^{23}$ mol^{-1}), and the molar weight of water ($M_w = 0.018$ kg mol^{-1}) according to Newman (1983) and Quirk and Murray (1999) as given in Equation 2:

$$SSA_w = \frac{\theta_0 \times N_a \times A}{M_w} \quad (2)$$

2.4 | Numerical and statistical analysis

The linear relation between two variables was determined by least-squares regression as implemented in MATLAB (The MathWorks, 2018). The goodness of fit was assessed by the coefficient of determination, R^2, and the RMSE, as given in Equation 3:

$$RMSE = \sqrt{\sum_{i=1}^{n} \frac{(\hat{y}_i - y_i)^2}{n}} \quad (3)$$

where n is the number of observations, and y_i and $\hat{y}_i$ are the ith observation and ith predicted value, respectively. The linear correlation between two variables was given as the Pearson linear correlation coefficient r.

The nonlinear least-squares regression to fit the Guggenheim–Anderson–de Boer model to the WSIs was performed using the trust–region–reflective algorithm as implemented in MATLAB and Optimization Toolbox (The MathWorks, 2018).

The significance of differences in means was assessed by ANOVA, and the post-hoc pairwise comparisons by Tukey's HSD test (Tukey, 1977).

TABLE 1 Physical and chemical properties. Texture classes according to Soil Survey Division Staff (1999)

Sample	Class	Clay[a]	fSilt[b]	cSilt[c]	Organic matter	SSA_{EGME}	CEC	EC	pH_w	pH_{CaCl_2}	Volume
		kg kg^{-1}				m^2 g^{-1}	cmol kg^{-1}	µS cm^{-1}	H^+		$\times 10^3$ m^3
AT	L	0.21	0.23	0.12	nd	31.90	8.52	12.01	7.19	6.05	1400
EI	SiL	0.16	0.37	0.16	0.002	22.68	6.04	7.23	6.39	4.91	nd
FB	L	0.24	0.27	0.16	nd	34.36	6.66	18.96	7.17	6.12	nd
IK-1	SiCL	0.40	0.40	0.09	nd	51.90	11.35	21.10	7.35	6.31	175
IK-2	SiL	0.19	0.45	0.15	0.005	33.38	7.55	12.73	6.36	4.85	250
IK-3	L	0.22	0.32	0.17	0.002	32.69	7.16	17.67	7.48	6.16	290
IK-4	SiCL	0.34	0.40	0.10	nd	48.67	9.21	15.34	7.27	6.02	360
NA-1	SiL	0.19	0.35	0.16	0.006	24.46	6.90	8.63	5.56	4.52	nd
NA-2	L	0.13	0.20	0.18	nd	17.21	4.25	10.77	6.40	5.10	nd
NU	SL	0.16	0.16	0.11	nd	43.34	9.92	9.93	7.38	6.15	140
QE	L	0.11	0.22	0.16	0.012	13.32	5.43	6.61	5.61	4.63	nd
QI-1	L	0.24	0.30	0.19	nd	43.26	7.97	13.19	7.16	6.05	nd
QI-2	L	0.26	0.22	0.16	0.001	27.93	14.25	58.10	6.70	6.26	200
QI-3	C	0.57	0.20	0.09	nd	88.60	21.91	10.02	7.53	5.95	nd
QI-4	CL	0.30	0.20	0.15	0.002	21.95	7.11	89.10	6.73	6.26	60
SQ	SiCL	0.40	0.42	0.01	0.012	24.09	9.25	2204.00	6.71	6.48	nd

Note. AT, Ataarnasit; C, clay; CEC, cation exchange capacity; CL, clay loam; EC, electrical conductivity; EI, Eqaluit Ilulat; FB, Fox Bay; IK, Iterlak; NA, Narsarsuaq; nd, below detection limit or not determined; NU, Nunakullak; QE, Qeqertaasaq; QI, Quinngua; SiCL, silty clay loam; SiL, silty loam; L, loam; SL, sandy loam; SQ, Sioraq; SSA_{EGME}, specific surface area determined by the standard EGME-method (ethylene glycol monomethyl ether). Volumes estimated from drone pictures.

[a]Clay, <2 µm.

[b]fSilt, 2–20 µm.

[c]cSilt, 20–50 µm.

3 | RESULTS AND DISCUSSION

3.1 | Identification and sampling of the GRF deposits

Figure 2 shows the map of the investigated area and the identified deposits. Some of the deposits were only accessible by water because of the lack of terrestrial infrastructure in Greenland caused by the rugged terrain. The area was dominated by the three major fjord systems: Bredefjord, Eriksfjord, and Einarsfjord (from north to south). A typical GRF deposition is shown in the photograph insert in Figure 2 (site AT); the overlying coarser sediments bearing the vegetation cover protecting the GRF from very fast erosion can be clearly identified. Generally, the probability of finding GRF decreased with increasing distance to the current ice margin, which could be explained with longer exposure to erosion of the outer-fjord deposits.

In the field, the texture of the deposits was assessed by feel partly following Thien (1979). Sediments with high fine particle content were sampled and brought to the laboratory for further analysis; sediments with high sand content were discarded (red crosses on the map in Figure 2). The GRF deposits were generally overlain by sand and gravel, which was removed prior to sampling; ~2 kg of field moist material was collected from a depth of ~30 cm from each deposit and stored in plastic bags.

In total, 16 from 32 investigated deposits with acceptable levels of fine particle content were retained and further analyzed in the laboratory (green squares in Figure 2). The different deposits were named according to local place names: SQ, Sioraq; QE, Qeqertaasaq; EI, Eqaluit Ilulat; NU, Nunakullak, QI-1 to QI-4, Quinngua; NA-1 and NA-2, Narsarsuaq; AT, Ataarnasit; FB, Fox Bay; and IK-1 to IK-4, Iterlak. The volumes of selected deposits were approximated from georeferenced aerial (drone) photographs and ranged from 60,000 m^3 (QE) to 1,400,000 m^3 (AT) with a median value of 225,000 m^3 (see Table 1).

In 2014, the total cultivated area in Greenland was ~1,100 ha (Lehmann et al., 2016) and the total estimated volume of selected deposits amounted to 2,875 $\times$ 10^3 m^3, which would be enough to cover the entire cultivated area with a theoretical surface application height of 25 cm.

3.2 | Grain geometry and mineralogy

The shape of the natural, untreated material was found to be mostly angular as shown in the example micrograph for

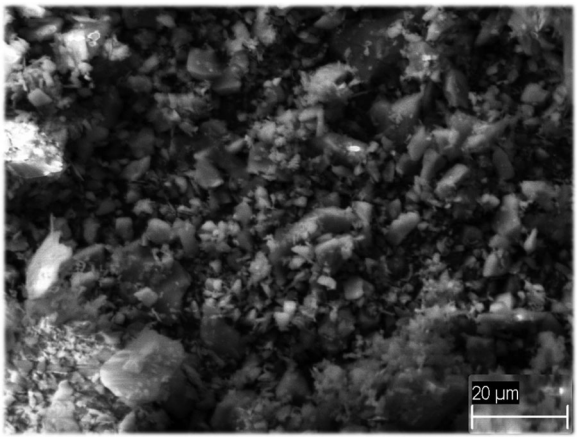

FIGURE 3 Scanning electron microscopy micrographs of sample Iterlak (IK-4)

sample IK-4 in Figure 3. This was expected because the crystal structure of the material was not altered during the physical weathering. The disintegration into smaller fragments happened along the cleavage planes, partly reflecting the shape of the unit cell crystal structure of the basic material. The X-ray diffraction analysis revealed that feldspars dominated the mineral composition of the sediments. The feldspars crystallize in mono- and triclinic crystal structures, exhibiting relatively sharp edges and plane surfaces (Smith & Brown, 1988). The resulting particles followed the shape of the unit cell crystal structure resulting in generally angular shapes.

Figure 4 a shows a typical diffractogram of a GRF exemplified by sample QI-3, the full-pattern Rietveld fit, and the resulting error in the bottom subplot. Supplemental Figure S1 shows the diffractograms of the 16 GRFs individually, and Supplemental Table S1 shows the relative abundance of the primary minerals following the Rietveld refinement.

The mineral assemblage of the sediments was dominated by feldspars (anorthite, oligoclase, and microcline, 72.5 ± 3.7%) and quartz (14.4 ± 4.1%); additionally, diffraction peaks of amphiboles (hornblende and arfvedsonite, 6.3 ± 1.4%) and micas (biotite and muscovite, 6.9 ± 2.0%) were identified and common to all of the 16 GRF samples. The origin of the broad hump at low diffraction angles (range 5–20° 2θ) was not clearly identified; it was either an instrument artifact or the result of the presence of nonidentified amorphous phases.

The similarity between the mineral assemblages of the 16 GRF deposits indicated common parent material (see Supplemental Table S1). The results were in accordance with the primary mineral compositions reported by Belmonte (2015) who also reported the presence of clay minerals associated to the chlorite–vermiculite group as well as illite and kaolinite for a GRF deposit sampled near Narsaq (see map in Figure 2). Generally, Belmonte (2015) and Pederstad and Jørgensen (1985) found high abundance of feldspars and quartz in the clay fraction (<2 µm), which indicated intense mechanical weathering.

3.3 | Texture and surface properties

The gravimetric clay content varied greatly among the 16 GRFs. The samples were identified as loamy sediments with generally high silt-to-clay content according to Soil Survey Division Staff (1999). The OM content were low to null (below detection limit).

The EC clearly reflected that the sediments were non-saline, except for sample SQ, which could be classified as very slightly saline according to Soil Survey Division Staff (1993). The pH values in water and $CaCl_2$ suggested slightly to moderately acidic conditions. The measured SSA_{EGME} of the GRFs were markedly lower than those reported for agriculturally used soils from Denmark (DSL) (Hansen, 1976; Resurreccion et al., 2011), exhibiting similar gravimetric clay and OM content. As a reference, soils from the DSL exhibiting OM <1.2% (13 soils) were plotted together with the GRFs in Figure 5a and b.

The total CEC of the GRFs was generally lower than those of agriculturally used soils exhibiting similar texture and OM content (Figure 5b). The SSA_{EGME} and the CEC correlated well with the gravimetric clay content ($r = .77$ and $r = .80$ for the SSA_{EGME} and CEC, respectively). Simple linear regressions yielded satisfactory results; the regression equations are given in the plot areas of Figure 5. Similar linear correlations between SSA_{EGME} and gravimetric clay content were reported by other studies, although the linear dependence of SSA_{EGME} on the gravimetric clay content was generally stronger (e.g., Petersen et al., 1996). Omitting sample QI-3, the correlation coefficients and significance levels (p values) between gravimetric clay content and SSA_{EGME} and CEC dropped to $r = .49$, $p = .049$ and $r = .57$, $p = .028$, respectively. The CEC was positively correlated to the SSA_{EGME} ($r = .83$), similar to the findings of Curtin and Smillie (1976) and Petersen et al. (1996).

3.4 | Extended physical characterization using laser diffraction

Figure 6a exemplifies the PSD measured by laser diffraction (LD, solid lines) and conventionally by a combination of the sieve and pipette (SP) methods (filled squares). The multimodality of the PSD of the GRFs was well depicted by the frequency distribution (FD) determined by LD (FD_{LD}).

The first and second modes occurred within the narrow size ranges around a mean value of 4.02 ± 1.17 and 27.82 ± 12.78 µm (sample SQ excluded), respectively. The particle size distributions of the different GRFs were thus very

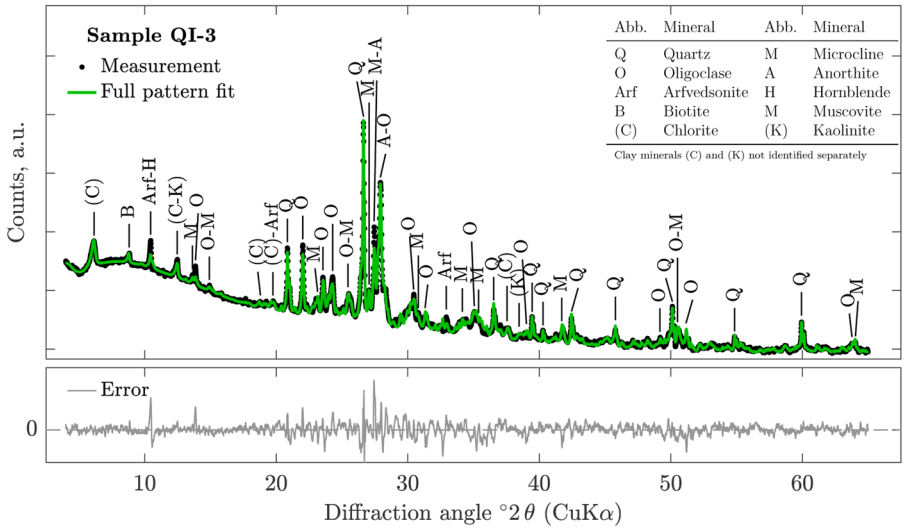

FIGURE 4 Example X-ray diffraction diffractogram for sample Quinngua (QI)-3. Counts per second (black dots) and Rietveld fit (green) and the corresponding error (grey) in the bottom subplot. The phyllosilicates chlorite (C) and kaolinite (K) were not identified separately on the <2-μm fraction, but their potential diffraction peaks were indicated

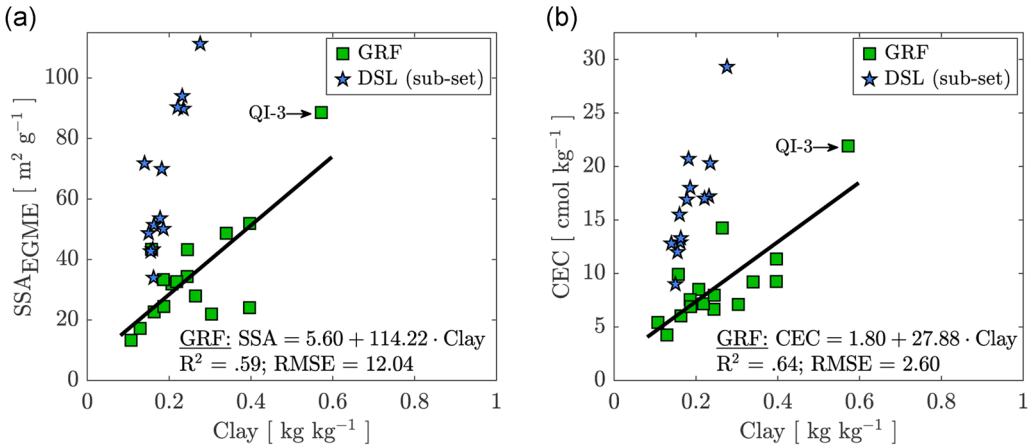

FIGURE 5 (a) Specific surface area (SSA_{EGME}) ($m^2\ g^{-1}$) and (b) cation exchange capacity (CEC) ($cmol\ kg^{-1}$) of the glacial rock flours (GRFs) as a function of the gravimetric clay. A subset of the Danish soil library dataset (DSL) (13 out of 41 soils) with similar clay and organic matter content was added for reference

similar in terms of their principal mode locations (first and second modes). The individual PSDs of all the GRFs are shown in Supplemental Figure S2. Figure 6b shows the PSD_{LD} of all the 16 GRFs measured by LD. The smallest particle diameter averaged over all the samples was detected at d_{min} = 0.60 ± 0.08 μm, sample QI-3 excluded (d_{min} = 0.07 μm).

In this study, the relationship between the conventionally determined gravimetric clay fraction (Clay) and the volumetric fraction <2 μm, $F(d < 2\ \mu m)$, determined by LD could be described by Clay = 0.02 + 2.57 × $F(d < 2\ \mu m)$, with R^2 = 0.68 and RMSE = 0.07 (data not shown), and was in the same order of magnitude as the findings of Konert and Vandenberghe (1997), for example, although the relationship found in this study exhibited lower goodness of fit.

The gravimetric clay content was best represented by the volumetric fraction of particles exhibiting a diameter <3.38 μm as shown in Figure 7a; it was reasonably close to the first mode of the FD_{LD} as derived earlier (d = 4.02 μm). As shown in Figure 7, the volumetric fraction of particles with diameter <2.38 μm was an excellent predictor of the SSA_{EGME} and the CEC, exhibiting coefficients of determination (R^2) of .89 and .81, respectively.

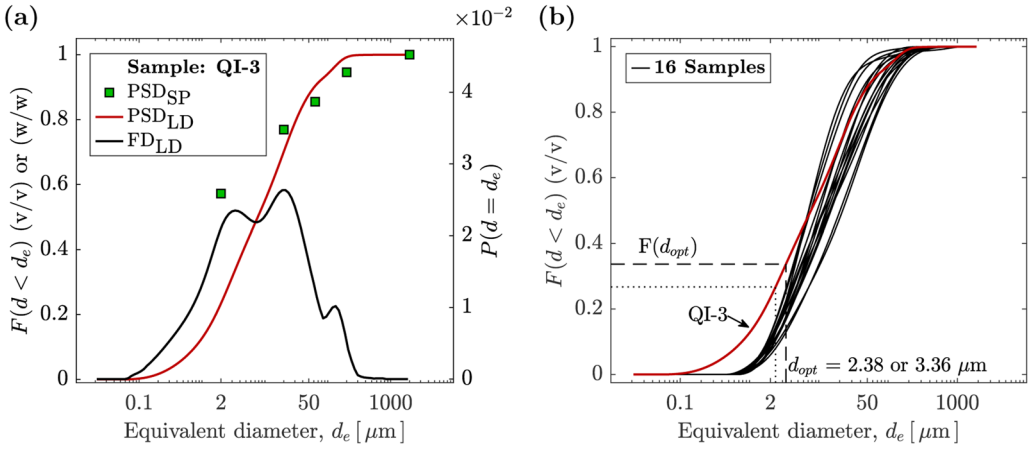

FIGURE 6 (a) Combined plot of the particle size distribution (PSD) measured by laser diffraction (LD, solid lines) and sieve and pipette (SP, filled squares); the cumulative particle size distributions (PSD_{SP} and PSD_{LD}) and the frequency distribution (FD_{LD}), exemplified by sample Quinngua (QI)-3. (b) PSD_{LD} of the 16 glacial rock flours and indicated volumetric fraction, $F(d_{opt})$, at d_{opt} = 2.38 μm and d_{opt} = 3.36 μm shown explicitly for the sample QI-3 by the dashed lines

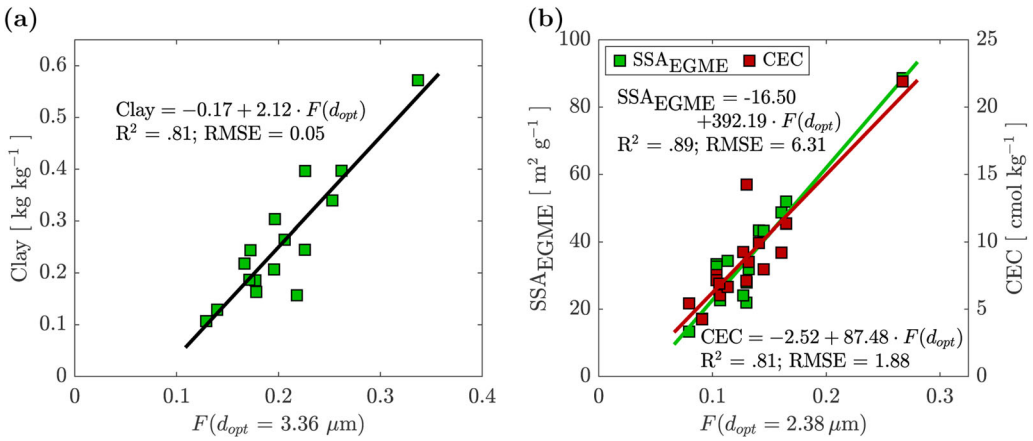

FIGURE 7 (a) Best agreement between particle size distribution measured by laser diffraction (PSD_{LD}) fraction and gravimetric clay determined conventionally (found at d_{opt} = 3.36 μm, based on minimum RMSE) and the best-fit line. (b) Best agreement between PSD_{LD} fraction and specific surface area determined by the standard EGME-method (ethylene glycol monomethyl ether) (SSA_{EGME}) or cation exchange capacities (CEC) (found at d_{opt} = 2.38 μm)

3.5 | Extended physical characterization using water vapor sorption

The WSIs determined on the GRFs exhibited minimum and maximum equilibrium RH between 7.2 ± 5.7 and 92.6 ± 0.3%, corresponding to a soil-water potential (ψ) range of −360 to −10 MPa. Besides samples SQ and QI-3, the WSIs of the GRFs shared similar geometry with a relatively low degree of hysteresis as shown in Figure 8a. The individual sorption isotherms are shown in Supplemental Figure S3. The distinct shape of both ad- and desorption isotherms of sample SQ could be explained by the salinity, that is, the relatively high EC compared with the other samples (Chen et al., 2020). The generally higher θ_m throughout the whole RH range of sample QI-3 could be attributed to the significantly higher clay content. No apparent correlation between the mineralogy and the shape or θ_m level of the WSIs could be found.

Figure 8b, c, and d show the WSIs of selected GRFs compared with agriculturally used soils in which the gravimetric clay fraction was dominated by either montmorillonite (MO), illite (IL), or kaolinite (KA). The comparative soil samples were taken from Arthur et al. (2020) and selected such that the soil samples exhibited clay content as close as possible to the minimum (b), median (c), and maximum (d) clay content of the GRFs. The WSIs of the GRFs closely followed the ones of the KA-soils for RH <80%. For the given RH ranges, the water content of the 2:1 clays (IL and MO) were considerably higher.

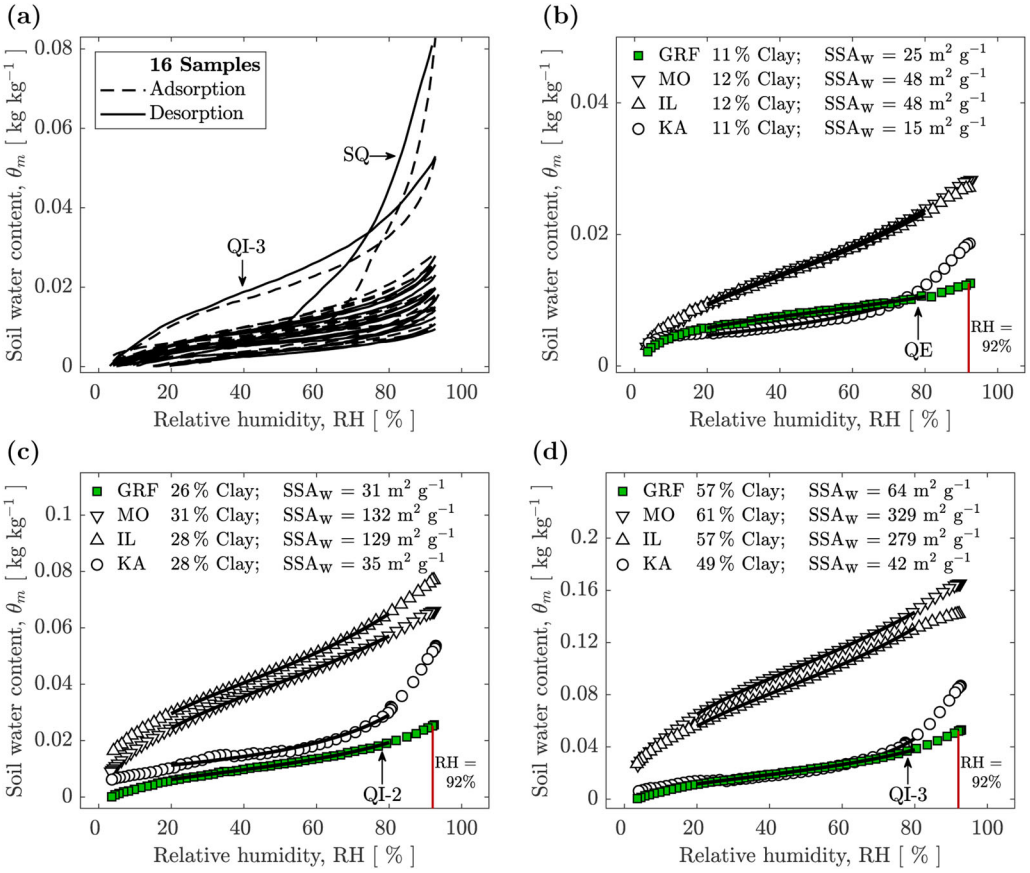

FIGURE 8 (a) Water vapor sorption isotherms of the 16 glacial rock flours (GRFs). Desorption isotherms for (b) low, (c) median, and (d) high clay-level GRFs (green filled squares) and soils bearing similar levels of montmorillonitic (MO), illitic (IL), and kaolinitic (KA) dominated clay content. Fitted Guggenheim–Anderson–de Boer (GAB) model (solid black lines). The red vertical line indicates the water content at relative humidity (RH) = 0.92 ($\psi \approx -11$ MPa). Some isotherms were partly hidden by others. Note the differences in *y* axis limits

The estimated SSA_w of the GRFs were in line with the SSA_w of the KA-soils. The IL- and MO-soils exhibited, as expected, significantly larger surface areas for given clay content. For reference, the slopes of the trend lines were given in the plot area of Figure 9a. As reported by other studies (Akin & Likos, 2014; Arthur et al., 2018), the SSA_w and the SSA_{EGME} were significantly correlated; a linear regression, excluding the sample SQ, exhibited acceptable goodness of fit (Table 2). However, considering only the KA-soils from Arthur et al. (2020), the regression coefficients of the best fit line were very close to those obtained for the GRFs (Table 2).

3.6 | Towards soil amendment

A linear relationship between the water content at the permanent wilting point (PWP) at $\psi = -1.5$ MPa (RH = 98.9%) and the water content at RH = 92.1% (highest equilibrium RH of the WSIs common to all the GRFs) was established from measurements of the soil-water retention at low water content of the DSL-dataset (Resurreccion et al. (2011). The regression resulted in an excellent fit, with a coefficient of determination (R^2) of 0.96. The regression was not dependent on the OM content as shown in Figure 10a. Thus, the relationship could directly be used to estimate the PWP of the GRFs and the Arthur et al. (2020) comparison soils. The PWPs of the DSL dataset were taken from the water-retention measurements directly.

Figure 10b clearly depicted the linear dependence of the PWP on the gravimetric clay content and the distinctively different relationship obtained for the GRFs, depicted by the substantially different slopes of the trend lines. The direct identification of the reason for the considerably different behavior was hidden by the effect of the OM on the PWP of the comparison soils.

To investigate the effect of GRF on the plant available water (PAW) content, we amended a sandy soil from South Greenland (clay, 1.33%; OM, 2.33%) with four levels of GRF from deposit QI-3 (0, 5, 10, and 15% w/w). For each binary mix, we repacked five replicates into soil-core cylinders (diam., 60.5 mm; height, 34.8 mm; volume, 100 cm^3) to a dry bulk density of 1.4 Mg m^{-3}. The samples were saturated in a retention box and equilibrated to $\psi = -100$ hPa corresponding to

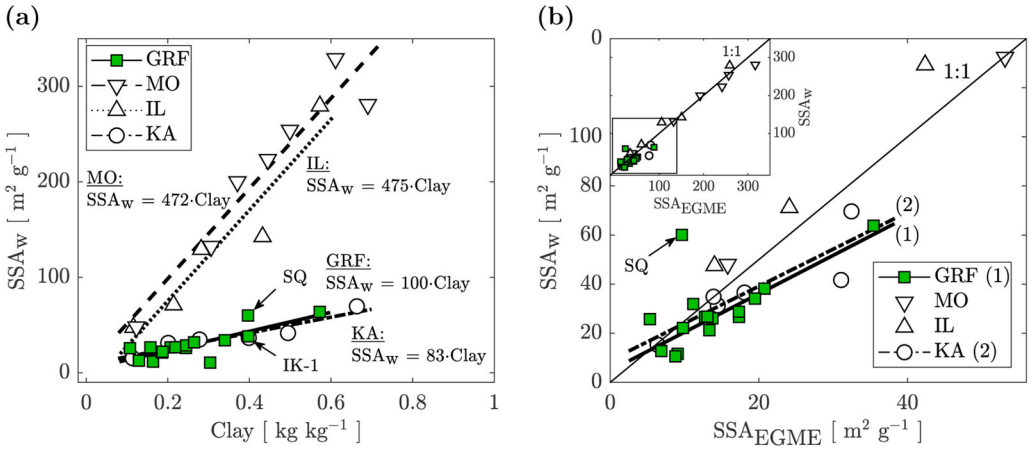

FIGURE 9 Properties determined on the water-vapor sorption isotherms. (a) Specific surface area estimated from water vapor sorption isotherms (SSA_w) as a function of gravimetric clay content and trend lines for the four different materials (only slope of the trend line given as reference); (b) SSA_w vs. the specific surface area determined by the standard EGME method (SSA_{EGME}) and the best fit line of the glacial rock flours (GRFs) (excluding sample SQ) and the kaolinite (KA) soils (see Table 2)

TABLE 2 Regression equations and goodness of fit for Figure 9b. Result of regression for combined illitic (IL) and montmorillonitic (MO) soils given for completeness

Reference	Material	Regression equation	R^2	RMSE
				$m^2\ g^{-1}$
(1) Figure 9b	GRF (− site SQ)	$SSA_w = 4.79 + 0.63 \times SSA_{EGME}$	.80	5.94
(2) Figure 9b	KA	$SSA_w = 8.79 + 0.60 \times SSA_{EGME}$	.76	9.65
(−) Figure 9b	IL + MO	$SSA_w = 20.50 + 0.88 \times SSA_{EGME}$	.98	14.33

Note. GRF, glacial rock flour; KA, kaolinitic clay dominated soils; SQ, Sioraq; SSA_w, specific surface area estimated from water vapor sorption isotherms; SSA_{EGME}, specific surface area determined by the standard ethylene glycol monomethyl ether method.

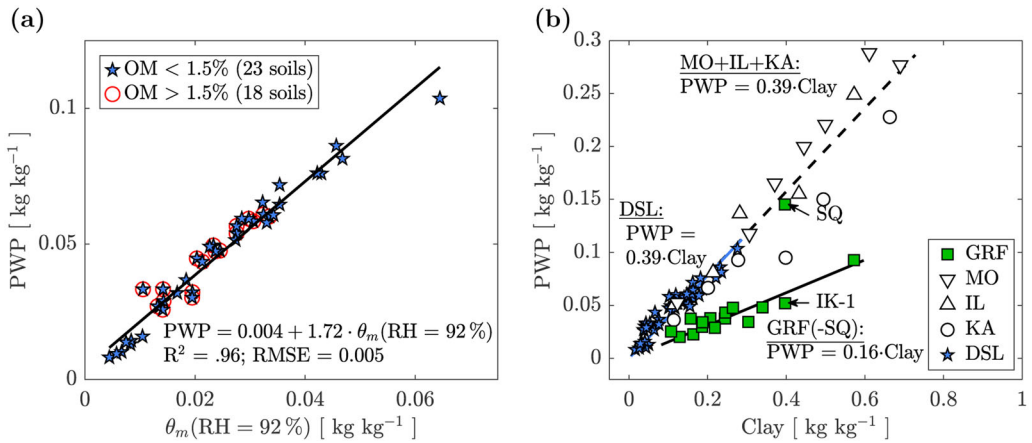

FIGURE 10 (a) Estimation of water content at the wilting point (PWP) based on the Danish soil library dataset (DSL, 41 soils), and (b) linear relation between PWP and gravimetric clay of the glacial rock flours (GRFs) and comparison soils. IL, illitic; KA, kaolinitic; MO, montmorillonitic; OM, organic matter; RH, relative humidity

the field capacity of sandy soils (Aljibury & Evans, 1965). We estimated the PWP of the binary mixtures from the clay content, according to Hansen (1976) (PWP = 0.336 × clay + 0.973, based on 209 Danish soils). The PAW was then calculated as the difference between water content at field capacity and the PWP. Figure 11 shows the resulting mean PAW for each GRF concentration. The one-way ANOVA revealed that there was a significant effect at the $p < .05$ level of

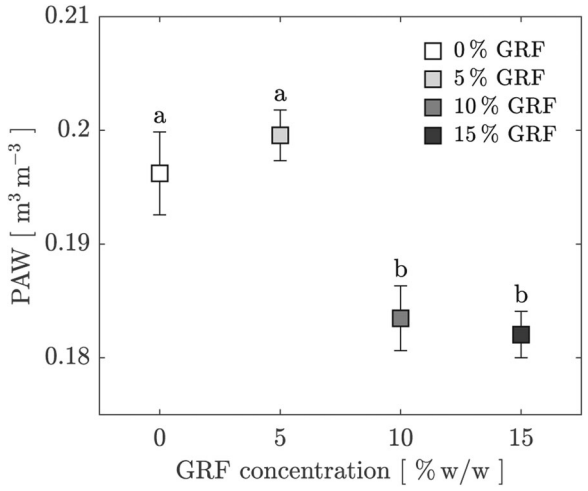

FIGURE 11 Plant available water (PAW) of a repacked, glacial rock flour (GRF) amended, sandy soil from Greenland. Symbols (mean PAW values) bearing the same letters are not statistically significant form each other. The whiskers represent the standard deviation

the GRF concentration on the PAW [$F(3,16) = 51.3$, $p < .001$]. The post-hoc pairwise comparisons (Tukey's HSD test) are displayed by letter notation in Figure 11. Although not statistically significant, the addition of 5% GRF showed a tendency for PAW increase. The reduction in PAW for the two highest GRF concentrations vs. the 0 and 5% levels mainly were due to lower water content at field capacity resulting from a reduction of meso-sized pores because of a shift in the PSD.

Figure 12a gives the overview of the CEC measurements obtained for the different materials as a function of the gravimetric clay content. The CEC of pure MO (100 cmol kg^{-1}) and pure KA (5 cmol kg^{-1}) (Carroll, 1959) were added as a visual guide. According to Schnitzer (1965), the OM contributes significantly (30–60%) to the CEC; although exhibiting higher OM content, the CEC of the KA-soils (mean OM, 0.5%) were generally lower than the CEC of the GRFs (mean OM, 0.3%). The presence of 2:1 clay minerals and micas in the mineral composition were likely the reason for the slightly higher CEC (Carroll, 1959). Belmonte (2015) found high content of primary minerals in the clay-sized fraction of comparable sediments, which explained the lower CEC than the IL- and MO-soils for given clay content.

The SSC of the GRFs were similar to or slightly higher than the SSC of comparable soils exhibiting low OM content. As a reference, all the soils from the DSL were added to Figure 12b; samples exhibiting OM > 1.5% were highlighted by red circles to expose the paramount influence of the OM on the SSC.

4 | CONCLUSIONS

The study characterized 16 GRF deposits located across South Greenland in the perspective of their suitability as soil conditioner for the local farmland. From the results, we conclude the following:

(1) Based on the estimated volumes of the GRF deposits, the exploitation for local agricultural use should be feasible. The deposits QI-3, AT, and IK-4, close to major agricultural areas, are easily accessible and high in clay content (0.21–0.57 kg kg^{-1}) and thus well suited for exploitation.
(2) The scanning electron microscopy micrographs showed that the particles were mostly angular in shape.
(3) The X-ray diffractograms revealed that the GRF shared similar mineralogies and contained large fractions of primary minerals (quartz and feldspars).
(4) The LD granulometry revealed the multimodality of the PSDs; the surface properties (SSA_{EGME} and CEC) of the GRFs could be accurately predicted by LD-determined volumetric fractions of particles exhibiting a diameter <2.38 µm.
(5) The GRF exhibited low water vapor sorption, comparable with soils dominated by kaolinitic clay and much lower compared with 2:1 clay-dominated soils. For given clay content, the SSA_{EGME} and the SSA_{w} were in line with KA-dominated soils.
(6) The water content at the PWP of Greenlandic soils is unlikely to be increased by the addition of GRF because of the low sorption activity.
(7) Five percent GRF addition to a sandy, cultivated soil from South Greenland showed a tendency to increase PAW content, whereas very high amendments of 10–15% decreased PAW.
(8) Despite the lack of OM, the GRF exhibited relatively high CEC and SSC compared with soils dominated by KA-clay.

This study showed promising results in view of the use of GRF as a soil conditioner and amendment for sandy agricultural soils in South Greenland. It is likely that GRF amendment reduces water repellency in a relatively short period of time and increases the soil's nutrient holding capacity.

Future research should investigate the long-term effect of GRF amendment on soil aggregation potential and water-holding capacity of sandy and structurally low developed subarctic agricultural soils. In perspective, to give local farmers advice on application rates and suitable soils for GRF amendment, field-plot experiments covering the major soil types in Greenland are necessary.

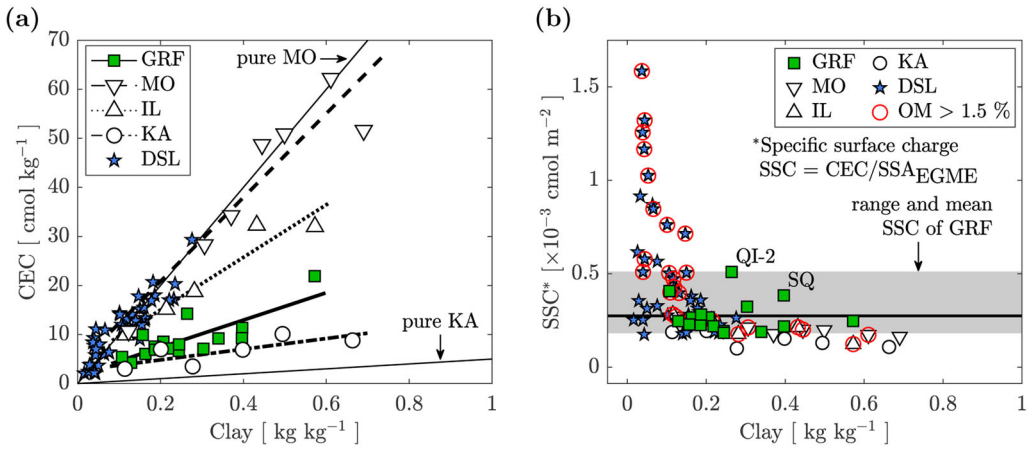

FIGURE 12 (a) Cation exchange capacity (CEC) of the three used datasets vs. gravimetric clay. The two solid black lines indicate the CEC levels of pure kaolinite (KA) (5 cmol kg^{-1}) and montmorillonite (MO) (100 cmol kg^{-1}). (b) Specific exchangeable surface charge (SSC = CEC/specific surface area [SSA]) of the three datasets as a function of gravimetric clay

ACKNOWLEDGMENTS

The research was financed by the Danish Council for Independent Research, Technology, and Production Sciences via the project "Glacial Flour as a New, Climate-Positive Technology for Sustainable Agriculture in Greenland: NewLand." We would like to thank Donghong Yu (Aalborg University, Department of Chemistry and Bioscience) and Thomas Sørensen Quaade (Aalborg University, Department of Materials and Production) for providing access to the XRD and for the help with the SEM, respectively. We also would like to thank the editor and reviewers for their valuable comments to improve the quality of the paper.

AUTHOR CONTRIBUTIONS

Charles Pesch: Conceptualization; Data curation; Formal analysis; Investigation; Methodology; Resources; Validation; Visualization; Writing-original draft; Writing-review & editing. Peter Lystbæk Weber: Conceptualization; Data curation; Formal analysis; Investigation; Methodology; Resources; Validation. Per Moldrup: Conceptualization; Data curation; Formal analysis; Funding acquisition; Investigation; Methodology; Project administration; Resources; Supervision; Validation; Writing-review & editing. Lis de Jonge: Conceptualization; Data curation; Funding acquisition; Methodology; Project administration; Resources; Supervision; Writing-review & editing. Emmanuel Arthur: Conceptualization; Data curation; Formal analysis; Investigation; Methodology; Resources; Validation; Writing-review & editing. Mogens Humlekrog Greve: Conceptualization; Funding acquisition; Investigation; Project administration; Validation; Writing-review & editing.

CONFLICT OF INTEREST

The authors report no conflicts of interest.

ORCID

Charles Pesch https://orcid.org/0000-0003-4120-0239
Peter Lystbæk Weber https://orcid.org/0000-0001-9249-0796
Per Moldrup https://orcid.org/0000-0003-1619-1457
Lis Wollesen de Jonge https://orcid.org/0000-0003-2874-0644
Emmanuel Arthur https://orcid.org/0000-0002-0788-0712
Mogens Humlekrog Greve https://orcid.org/0000-0001-9099-8940

REFERENCES

Akin, I. D., & Likos, W. (2014). Specific surface area of clay using water vapor and EGME sorption methods. *Geotechnical Testing Journal*, *37*, 1016–1027. https://doi.org/10.1520/GTJ20140064

Aljibury, F. K., & Evans, D. D. (1965). Water permeability of saturated soils as related to air permeability at different moisture tensions. *Soil Science Society of America Journal*, *29*, 366–369. https://doi.org/10.2136/sssaj1965.03615995002900040008x

Andrews, J. T. (2011). Unraveling sediment transport along glaciated margins (the Northwestern Nordic Seas) using quantitative X-ray diffraction of bulk (2 mm) sediment. In F. Bhuiyan (Ed.), *Sediment transport* (pp. 225–248). IntechOpen.

Arthur, E., Tuller, M., Moldrup, P., & de Jonge, L. W. (2014). Evaluation of a fully automated analyzer for rapid measurement of water vapor sorption isotherms for applications in soil science. *Soil Science Society of America Journal*, *78*, 754–760. https://doi.org/10.2136/sssaj2013.11.0481n

Arthur, E., Tuller, M., Moldrup, P., & de Jonge, L. W. (2020). Clay content and mineralogy, organic carbon and cation exchange capacity affect water vapour sorption hysteresis of soil. *European Journal of Soil Science*, *71*, 204–214. https://doi.org/10.1111/ejss.12853

Arthur, E., Tuller, M., Moldrup, P., Greve, M. H., Knadel, M., & de Jonge, L. W. (2018). Applicability of the Guggenheim–Anderson–Boer water vapour sorption model for estimation of soil specific surface area. *European Journal of Soil Science*, *69*, 245–255. https://doi.org/10.1111/ejss.12524

Belmonte, L. J. (2015). *Use of Greenlandic resources for the production of bricks* (PhD thesis, Technical University of Denmark, Department of Civil Engineering).

Bennike, O., Björck, S., & Lambeck, K. (2002). Estimates of South Greenland late-glacial ice limits from a new relative sea level curve. *Earth and Planetary Science Letters*, *197*, 171–186. https://doi.org/10.1016/S0012-821X(02)00478-8

Bennike, O., Jensen, J. B., Næsby Sukstorf, F., & Rosing, M. T. (2019). Mapping glacial rock flour deposits in Tasersuaq, southern West Greenland. *GEUS Bulletin*, *43*. https://doi.org/10.34194/GEUSB-201943-02-06

Bentley, S. P., & Smalley, I. J. (1979). Mineralogy of a leda/champlain clay from Gloucester (Ottawa, Ontario). *Engineering Geology*, *14*, 209–217. https://doi.org/10.1016/0013-7952(79)90086-3

Berrangé, J. P. (1966). *The bedrock geology of Vatnahverfi, Julianehåb district, South Greenland*. Kobenhavn.

Besnard, E., Chenu, C., Balesdent, J., Puget, P., & Arrouyas, D. (1996). Fate of particulate organic matter in soil aggregates during cultivation. *European Journal of Soil Science*, *47*, 495–503. https://doi.org/10.1111/j.1365-2389.1996.tb01849.x

Carroll, D. (1959). Ion exchange in clays and other minerals. *GSA Bulletin*, *70*, 749–779. https://doi.org/10.1130/0016-7606(1959)70%5b749:IEICAO%5d2.0.CO;2

Caviezel, C., Hunziker, M., & Kuhn, N. J. (2017). Bequest of the Norseman—The potential for agricultural intensification and expansion in southern Greenland under climate change. *Land*, *6*, 87. https://doi.org/10.3390/land6040087

Chen, M., Zeng, W., Arthur, E., Gaiser, T., Lei, G., Zha, Y., Ao, C., Fang, Y., Wu, J., & Huang, J. (2020). Relating soil salinity, clay content and water vapour sorption isotherms. *European Journal of Soil Science*, *71*, 399–414. https://doi.org/10.1111/ejss.12876

Curtin, D., & Smillie, G. W. (1976). Estimation of components of soil cation exchange capacity from measurements of specific surface and organic matter. *Soil Science Society of America Journal*, *40*, 461–462. https://doi.org/10.2136/sssaj1976.03615995004000030041x

de Jonge, L. W., Jacobsen, O. H., & Moldrup, P. (1999). Soil water repellency: Effects of water content, temperature, and particle size. *Soil Science Society of America Journal*, *63*, 437–442. https://doi.org/10.2136/sssaj1999.03615995006300030003x

Dexter, A. R., Richard, G., Arrouays, D., Czyż, E. A., Jolivet, C., & Duval, O. (2008). Complexed organic matter controls soil physical properties. *Geoderma*, *144*, 620–627. https://doi.org/10.1016/j.geoderma.2008.01.022

Doebelin, N., & Kleeberg, R. (2015). Profex: A graphical user interface for the Rietveld refinement program BGMN. *Journal of Applied Crystallography*, *48*, 1573–1580. https://doi.org/10.1107/S1600576715014685

Gee, G. W., & Or, D. (2002). 2.4 particle-size analysis. In J. H. Dane & C. G. Topp (Eds.), *Methods of soil analysis: Part 4 physical methods, 5.4* (pp. 255–293). Soil Science Society of America. https://doi.org/10.2136/sssabookser5.4.c12

Gunnarsen, K. C. (2020). *Plant nutritional value of Greenlandic glacial rock flour: An amendment to improve weathered and nutrient poor soils* (PhD thesis, Department of Plant and Environmental Sciences, Faculty of Science, University of Copenhagen).

Gunnarsen, K. C., Jensen, L. S., Gómez-Muñoz, B., Rosing, M. T., & de Neergaard, A. (2019). Glacially abraded rock flour from Greenland: Potential for macronutrient supply to plants. *Journal of Plant Nutrition and Soil Science*, *182*, 846–856. https://doi.org/10.1002/jpln.201800647

Hansen, L. (1976). Jordtyper ved statens forsøgsstationer - Soil types at the Danish state experimental stations. Beretning fra statens forsøgsvirksomhed i plantekultur. (In Danish with English abstract) *Særtryk af Tidsskrift for Planteavl*, *80*, 742–758.

Henriksen, N. (2008). *Geological history of Greenland: Four billion years of earth evolution*. Geological Survey of Denmark and Greenland (GEUS).

Jakobsen, B. H. (1991). Multiple processes in the formation of subarctic podzols in Greenland. *Soil Science*, *152*, 414–426. https://doi.org/10.1097/00010694-199112000-00003

Kalsbeek, E., Larsen, L. M., & Bondam, J. (1990). *Descriptive text to 1:500000 sheet 1, Sydgrønland*. Grønlands Geologiske Undersøgelse.

Karup, D., Moldrup, P., Tuller, M., Arthur, E., & de Jonge, L. W. (2017). Prediction of the soil water retention curve for structured soil from saturation to oven-dryness. *European Journal of Soil Science*, *68*, 57–65. https://doi.org/10.1111/ejss.12401

Kirschbaum, M. U. F. (1995). The temperature dependence of soil organic matter decomposition, and the effect of global warming on soil organic C storage. *Soil Biology and Biochemistry*, *27*, 753–760. https://doi.org/10.1016/0038-0717(94)00242-S

Konert, M., & Vandenberghe, J. (1997). Comparison of laser grain size analysis with pipette and sieve analysis: A solution for the underestimation of the clay fraction. *Sedimentology*, *44*, 523–535. https://doi.org/10.1046/j.1365-3091.1997.d01-38.x

Lehmann, J. O., Sharif, B., Kjeldsen, C., Plauborg, F., Olesen, J. E., Mikkelsen, M. H., Aastrup, P., Wegeberg, S., Kristensen, T., & Greve, M. H. (2016). *Muligheder for klimatilpasning i landbrugserhvervet - status og handlemuligheder*. Technical report. (In Danish) Aarhus Universitet, Institut for Agroøkologi/Naalakkersuisut: The Government of Greenland.

Maslov, B. S. (Ed.). (2009). *Agricultural land improvement: Amelioration and reclamation - Volume II*. EOLSS publications.

MATLAB and Optimization Toolbox (2018). *MATLAB and Optimization Toolbox, version 9.5.0 (R2018b)*. The MathWorks Inc.

Matus, F. J. (2021). Fine silt and clay content is the main factor defining maximal C and N accumulations in soils: A meta-analysis. *Scientific Reports*, *11*, 6438. https://doi.org/10.1038/s41598-021-84821-6

McKissock, I., Gilkes, R. J., & Walker, E. L. (2002). The reduction of water repellency by added clay is influenced by clay and soil properties. *Applied Clay Science*, *20*, 225–241. Clay Research in Australia and New Zealand. https://doi.org/10.1016/S0169-1317(01)00074-6

Nelson, D. W., & Sommers, L. E. (1996). Total carbon, organic carbon, and organic matter. In D. L. Sparks, A. L. Page, P. A. Helmke, & R. H. Loeppert (Eds.), *Methods of soil analysis: Part 3 chemical methods, 5.3* (pp. 961–1010). SSSA. https://doi.org/10.2136/sssabookser5.3.c34

Newman, A. C. D. (1983). The specific surface of soils determined by water sorption. *Journal of Soil Science*, *34*, 23–32. https://doi.org/10.1111/j.1365-2389.1983.tb00809.x

Nguyen, T.-T., & Marschner, P. (2013). Addition of a fine-textured soil to compost to reduce nutrient leaching in a sandy soil. *Soil Research*, *51*, 232–239. https://doi.org/10.1071/SR13105

Oades, J. M. (1984). Soil organic matter and structural stability: Mechanisms and implications for management. *Plant and Soil*, *76*, 319–337. https://doi.org/10.1007/BF02205590

Pederstad, K., & Jørgensen, P. (1985). Weathering in a marine clay during postglacial time. *Clay Minerals*, *20*, 477–491. https://doi.org/10.1180/claymin.1985.020.4.04

Pesch, C., Lamandé, M., de Jonge, L. W., Norgaard, T., Greve, M. H., & Moldrup, P. (2020). Compression and rebound characteristics of agricultural sandy pasture soils from South Greenland. *Geoderma*, *380*, 114608. https://doi.org/10.1016/j.geoderma.2020.114608

Pesch, C., Weber, P. L., de Jonge, L. W., Greve, M. H., Norgaard, T., & Moldrup, P. (2021). Soil–air phase characteristics: Response to texture, density, and land use in Greenland and Denmark. *Soil Science Society of America Journal*, *85*, 1534–1554. https://doi.org/10.1002/saj2.20284

Petersen, L. W., Møldrup, P., Jacobsen, O. H., & Rolston, D. E. (1996). Relations between specific surface area and soil physical and chemical properties. *Soil Science*, *161*, 9–12. https://doi.org/10.1097/00010694-199601000-00003

Pribyl, D. W. (2010). A critical review of the conventional SOC to SOM conversion factor. *Geoderma*, *156*, 75–83. https://doi.org/10.1016/j.geoderma.2010.02.003

Quirk, J. P., & Murray, R. S. (1999). Appraisal of the ethylene glycol monoethyl ether method for measuring hydratable surface area of clays and soils. *Soil Science Society of America Journal*, *63*, 839–849. https://doi.org/10.2136/sssaj1999.634839x

Ramesh, R., & D'Anglejan, B. (1995). Mineralogy, chemistry and particle size interrelationships in some post-glacial marine deposits of the St. Lawrence Lowlands. *Journal of Coastal Research*, *11*, 1167–1179.

Rawls, W. J., & Brakensiek, D. L. (1982). Estimating soil water retention from soil properties. *Journal of the Irrigation and Drainage Division*, *108*, 166–171. https://doi.org/10.1061/JRCEA4.0001383

Resurreccion, A. C., Moldrup, P., Tuller, M., Ferré, T. P. A., Kawamoto, K., Komatsu, T., & de Jonge, L. W. (2011). Relationship between specific surface area and the dry end of the water retention curve for soils with varying clay and organic carbon contents. *Water Resources Research*, *47*. https://doi.org/10.1029/2010WR010229

Rhoades, J. D. (1996). Salinity: Electrical conductivity and total dissolved solids. In D. L. Sparks, A. L. Page, P. A. Helmke, R. H. Loeppert, P. N. Soltanpour, M. A. Tabatabai, C. T. Johnston, & M. E. Sumner (Eds.), *Methods of soil analysis: Part 3 chemical methods, 5.3* (pp. 417–435). SSSA. https://doi.org/10.2136/sssabookser5.3.c14

Roaldset, E. (1972). Mineralogy and geochemistry of Quaternary clays in the Numedal area, southern Norway. *Norsk Geologisk Tidsskrift*, *52*, 335–369.

Ryżk, M., & Bieganowski, A. (2011). Methodological aspects of determining soil particle-size distribution using the laser diffraction method. *Journal of Plant Nutrition and Soil Science*, *174*, 624–633. https://doi.org/10.1002/jpln.201000255

Schjønning, P., de Jonge, L. W., Moldrup, P., Christensen, B. T., & Olesen, J. E. (2010). Searching the critical soil organic carbon threshold for satisfactory tilth conditions – test of the Dexter clay:carbon hypothesis. In *Proceedings of the 1st International conference and exploratory workshop on soil architecture and physico-chemical functions "Cesar"* (pp. 341–346). Aarhus University, Faculty of Agricultural Sciences.

Schnitzer, M. (1965). Contribution of organic matter to the cation exchange capacity of soils. *Nature*, *207*, 667–668. https://doi.org/10.1038/207667a0

Simonson, R. W. (1959). Outline of a generalized theory of soil genesis. *Soil Science Society of America Journal*, *23*, 152–156. https://doi.org/10.2136/sssaj1959.03615995002300020021x

Smith, J. V., & Brown, W. L. (1988). *Feldspar minerals vol. 1, crystal structure, physical, chemical and microtextural properties*. Springer.

Soil Survey Division Staff. (1993). *Soil survey handbook*. Agricultural Handbook 18. NRCS, USDA.

Soil Survey Division Staff (1999). *A basic system of soil classification for making and interpreting soil surveys*. Agricultural Handbook 436. NRCS, USDA.

Sukstorf, F. N., Bennike, O., & Elberling, B. (2020). Glacial rock flour as soil amendment in subarctic farming in South Greenland. *Land*, *9*, 198. https://doi.org/10.3390/land9060198

Sumner, M. E., & Miller, W. P. (1996). Cation exchange capacity and exchange coefficients. In D. L. Sparks, A. L. Page, P. A. Helmke, R. H. Loeppert, P. N. Soltanpour, M. A. Tabatabai, C. T. Johnston, & M. E. Sumner (Eds.), *Methods of soil analysis: Part 3 chemical methods, 5.3* (pp. 1201–1229). SSSA. https://doi.org/10.2136/sssabookser5.3.c40

Tahir, S., & Marschner, P. (2016). Clay amendment to sandy soil – effect of clay concentration and ped size on nutrient dynamics after residue addition of low C/N ratio residue. *Journal of Soil Science and Plant Nutrition*, *16*, 864–875. https://doi.org/10.4067/S0718-95162016005000061

Thien, S. J. (1979). A flow diagram for teaching texture-by-feel analysis. *Journal of Agronomic Education*, *8*, 54–55. https://doi.org/10.2134/jae.1979.0054

Thomas, G. W. (1996). Soil pH and soil acidity. In D. L. Sparks, A. L. Page, P. A. Helmke, R. H. Loeppert, P. N. Soltanpour, M. A. Tabatabai, C. T. Johnston, & M. E. Sumner (Eds.), *Methods of soil analysis: Part 3 chemical methods, 5.3* (pp. 475–490). SSSA. https://doi.org/10.2136/sssabookser5.3.c16

Tukey, J. W. (1977). *Exploratory data analysis*. Addison-Wesley.

van den Berg, C., & Bruin, S. (1981). Water activity and its estimation in food systems: Theoretical aspects. In L. B. Rockland & G. F. Stewart (Eds.), *Water activity: Influences on food quality* (pp. 1–61). Academic Press.

van Straaten, P. (2007). *Agroecology: The use of rocks for crops*. Enviroquest.

Wagner, S., Cattle, S. R., & Scholten, T. (2007). Soil-aggregate formation as influenced by clay content and organic-matter amendment. *Journal of Plant Nutrition and Soil Science*, *170*, 173–180. https://doi.org/10.1002/jpln.200521732

Weber, P. L., de Jonge, L. W., Greve, M. H., Norgaard, T., & Moldrup, P. (2020). Gas diffusion characteristics of agricultural soils from South Greenland. *Soil Science Society of America Journal*, *84*, 1606–1619. https://doi.org/10.1002/saj2.20114

Weber, P. L., Hermansen, C., Norgaard, T., Pesch, C., Moldrup, P., Greve, M. H., Müller, K., Arthur, E., & de Jonge, L. W. (2021). Moisture-dependent water repellency of Greenlandic cultivated soils. *Geoderma*, *402*, 115189. https://doi.org/10.1016/j.geoderma.2021.115189

Westergaard-Nielsen, A., Bjørnsson, A. B., Jepsen, M. R., Stendel, M., Hansen, B. U., & Elberling, B. (2015). Greenlandic sheep farming controlled by vegetation response today and at the end of the 21st Century. *Science of The Total Environment*, *512–513*, 672–681. https://doi.org/10.1016/j.scitotenv.2015.01.039

White, L. F., Bailey, I., Foster, G. L., Allen, G., Kelley, S. P., Andrews, J. T., Hogan, K., Dowdeswell, J. A., & Storey, C. D. (2016). Tracking the provenance of Greenland-sourced, Holocene aged, individual sand-sized ice-rafted debris using the Pb-isotope compositions of feldspars and 40Ar/39Ar ages of hornblendes. *Earth and Planetary Science Letters*, *433*, 192–203. https://doi.org/10.1016/j.epsl.2015.10.054

SUPPORTING INFORMATION

Additional supporting information may be found in the online version of the article at the publisher's website.

How to cite this article: Pesch, C., Weber, P. L., Moldrup, P., de Jonge, L. W., Arthur, E., & Greve, M. H. (2022). Physical characterization of glacial rock flours from fjord deposits in South Greenland–Toward soil amendment. *Soil Science Society of America Journal*, *86,*407–422. https://doi.org/10.1002/saj2.20352